# Transport through normal-metal–graphene contacts

Ya. M. Blanter
*Kavli Institute of Nanoscience, Delft University of Technology, Lorentzweg 1, 2628 CJ Delft, The Netherlands*

Ivar Martin
*Theoretical Division, Los Alamos National Laboratory, Los Alamos, New Mexico 87544, USA*
(Received 23 May 2007; published 25 October 2007)

Conductance of zigzag interfaces between a graphene sheet and a normal metal is investigated in the tight-binding approximation. Boundary conditions, valid for a variety of scattering problems, are constructed and applied to the normal-metal–graphene–normal-metal junctions. At the Dirac point, the conductance is determined solely by the evanescent modes and is inversely proportional to the length of the junction. It is also independent of the interface resistance. Away from the Dirac point, the propagating modes' contribution dominates. We also observe that even in the junctions with high interface resistance, for certain modes, ideal transmission is possible via Fabry-Pérot-like resonances.

DOI: 10.1103/PhysRevB.76.155433 PACS number(s): 73.23.Ad, 73.40.Cg, 73.40.Sx, 73.63.Rt

## I. INTRODUCTION

Recent experimental studies[1–4] uncovered unusual properties of graphene (graphite monolayers and bilayers), strongly contrasting with the common knowledge inherited from studies of metals. This difference originates from the fact that electrons in graphene monolayers obey the Dirac (rather than the Schrödinger) equation. Thus, one has an opportunity to study properties of the Dirac fermions in a tabletop experiment. Predictions of relativistic effects including the Klein tunneling[5] and *Zitterbewegung*[6] have been made. "Ordinary" phenomena, e.g., quantum Hall effect,[7] weak localization,[8] or Andreev reflection,[9] are also strongly modified in graphene as compared to normal metals.

The most easily accessible measurements in graphene are those of electrical transport. Theoretically, one way of understanding them is to extend the Landauer theory to graphene sheets, considering them as a junction between two reservoirs. So far, a common point was to describe reservoirs as bulk disordered graphene.[9–11] This approach considerably facilitates calculations; however, its relation to the experimental situation, with contacts made of normal metals, requires additional clarification. Indeed, the bulk in the available graphene devices is defect free.[12] Thus, the major source of electron scattering in graphene are the boundaries, in particular, contacts, and even a qualitative understanding of electric transport cannot be achieved without careful consideration of electron behavior in the contacts.

Experimentally, graphene flakes are contacted by tunnel junctions located on top of the flakes. Conceptually, we can discriminate between three types of junctions. One situation is when tunneling from the normal reservoir to graphene occurs just at one point, for instance, due to nonuniform thickness of the oxide layer in the contact in combination with the exponential dependence of the tunneling amplitude on this thickness. In this case, the voltage between the normal reservoir and the graphene sheet drops at the junction, and the chemical potential in graphene can be considered as fixed. For this pointlike tunneling, the resistance of a normal-metal–graphene–normal-metal (NGN) junction depends on the distance between the two tunneling points.

A different situation, apparently more experimentally relevant, is when tunneling occurs at many points, covering a large area (Fig. 1). In this case, there is no voltage drop on the contact, i.e., it becomes Ohmic. In the area under the contact, the wave functions of electrons from the normal reservoir and graphene quasiparticles hybridize, forming a substance which is a hybrid between graphene and normal metal. The nature of this substance depends on the exact properties of the contacts; however, it is reasonable to assume that, generally, it will be closer either to graphene or to a normal metal. In the former case, an effective description of a NGN system as a graphene-graphene-graphene (GGG) contact, where the voltage is applied to the graphene, is appropriate. In the latter case, the system is essentially a *planar* NGN junction, where the voltage is applied to the normal metal and drops at the interface between the normal metal and graphene. It is also clear that properties of such contacts considerably depend on the relation between lattice periods of graphene and normal metal, for instance, on whether the lattices are commensurate or not.

Below, we discuss the latter type of junctions—planar NGN junctions—to complement the earlier studies of GGG junctions. Recently, Schomerus[13] compared resistances of NGN contacts with a zigzag interface and GGG contacts. He considered the special case of equal overlap integrals between all neighboring sites in the tight-binding model. He found that if the graphene sheet is biased to the Dirac point, so that there are no propagating modes through graphene, the difference between NGN and GGG junctions is only quantitative. Outside this regime, the behavior of the contacts may strongly depend on the type of the leads and the interface. Below, we study this dependence for the simplest case of square-lattice leads and zigzag interfaces.

First, we consider within the tight-binding approximation the general problem of transmission through the NG interfaces and NGN structures for arbitrary overlap integrals $t_s$, $t_g$, and $t'$, in square-lattice normal metal, graphene, and at the interface, respectively. From the lattice Schrödinger equation, we derive the wave-function matching conditions at the

 

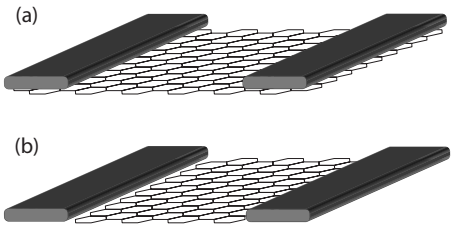


FIG. 1. (a) Typical experimental contact configuration: metallic leads overlaying graphene. The contact occurs over many microlinks, which leads to equilibration of the chemical potentials in the metal and in graphene. In the case of tight coupling under the contact, the band structures of graphene and the metal are expected to "fuse." (b) Theoretical model of a contact—tunneling between the metal leads and graphene zigzag edges. It can be thought of as a limiting case of strong coupling (a) with the tunable hybridization between contact and the edge.

interfaces. We apply them first to the scattering off the NG interface, and determine the reflection probability back to the normal metal.

Then, we turn to the conductance of a NGN junction. It is the sum of two contributions originating from propagating and evanescent modes in graphene. The number of the available propagating modes is proportional to the radius of the Dirac cone $q_G$ taken at the gate voltage energy $eV_G$, $q_G \propto V_G$. Their contribution to conductivity is therefore proportional to $V_G$; it is independent of the graphene length $L$ in the limiting cases $q_G L \ll 1$ and $q_G L \gg 1$. At the Dirac point ($V_G=0$), there are no propagating modes; however, there is a contribution to conductivity from the evanescent modes that obeys Ohm's law, i.e., is inversely proportional to the length of the graphene strip $L$.[11,13] For nonzero gate voltage $V_G$, the contribution of evanescent modes crosses over to $L^{-1}(q_G L)^{-3}$ behavior for $q_G L \gg 1$. We also observe that for the symmetric case $t'^2=t_s t_g$, a narrow graphene strip is ideally transmitting, both through the propagating and evanescent states. Moreover, the conductance of such a strip precisely at the Dirac point is independent of the interface overlap integral $t'$. Even for opaque interfaces, $t'^2 \ll t_s t_g$, we find that some modes transmit ideally, in direct analogy to the Fabry-Pérot resonances in double-barrier structure.

## II. NORMAL-METAL–GRAPHENE INTERFACE

We consider a zigzag interface between a normal metal with the square lattice and graphene with the bond lengths $a_s$ and $a_g$, matched such that $a_g=a_s/\sqrt{3}$, respectively (Fig. 2). We assume that the normal–metal band is taken near half-filling, so that the Fermi surface is nearly a square, whereas the graphene is tuned close to the Dirac point. In the normal metal, the wave functions are plane waves, $c(\boldsymbol{r})=(e^{ik_s x}+re^{-ik_s x})e^{ik_y y}$, $x<0$, defined on the sites of the square lattice. First and second terms describe incident and reflected waves, respectively. In graphene, one has to define two transmitted waves corresponding to two sublattices $a$ and $b$, $[d^a(\boldsymbol{r}),d^b(\boldsymbol{r})]$.

For the zigzag interface, the wave vector component along the interface $k_y$ is conserved, and thus, the two-

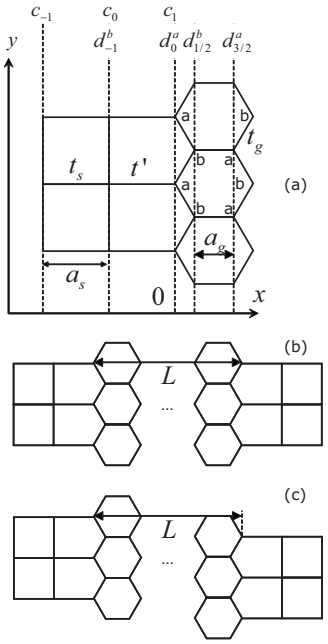


FIG. 2. (a) A zigzag interface between square and graphene lattices. Sites belonging to the two sublattices in graphene are indicated by $a$ and $b$. On the top, boundary conditions are sketched: We introduced two columns of fictitious amplitudes, $c_1$ in graphene and $d^b_{-1}$ in the square lattice, used them for wave-function matching at the interface. [(b) and (c)] A NGN contact of width $L=a_g(3N+1)/2$ with (b) an odd-integer or (c) an even-integer value of $N$.

dimensional scattering problem reduces to a collection of one-dimensional problems for different values of $k_y$. The transverse component of wave vector ($k_x$) is not conserved and must be found from the energy conservation.

In the tight-binding model, the amplitudes obey the lattice Schrödinger equation. In particular, at the interface, we obtain the following set of equations:

$$Ec_0 = -2t_s c_0 \cos k_y a_s - t_s c_{-1} - t' d^a_0,$$

$$Ed^a_0 = -t' c_0 - 2t_g \cos \frac{\sqrt{3}k_y a_g}{2} d^b_{1/2},$$

$$Ed^b_{1/2} = -t_g d^a_{3/2} - 2t_g \cos \frac{\sqrt{3}k_y a_g}{2} d^a_0, \quad (1)$$

where we moved to discrete notations (explained in Fig. 2): The subscript shows the distance from the interface, measured in corresponding lattice constants.

Away from the interface, the solution of the Schrödinger equation is a superposition of plane (or evanescent, see below) waves, with the energies

$$E_s = -2t_s(\cos k_s a_s + \cos k_y a_s),$$

$$E_g = \pm t_g \sqrt{1 + 4\cos\frac{\sqrt{3}k_y a_g}{2}\left(\cos\frac{\sqrt{3}k_y a_g}{2} + \cos\frac{3k_g a_g}{2}\right)}. \tag{2}$$

In this paper, we are mainly interested in the low-energy regime, $E \ll t_g$. In this regime, the energy can be expanded in the vicinity of the points where it turns to zero (the Dirac $K$ and $K'$ points), $k_g = q_x$, $k_y = \pm 4\pi/(3\sqrt{3}a_g) + q_y$, $E_\pm = \pm 3t_g q/2a_g$, with $q = (q_x^2 + q_y^2)^{1/2}$. For concreteness, we only consider the "upper" $K$ Dirac point, $k_y \approx 4\pi/3\sqrt{3}a_g$; by symmetry, the "lower" one, $K'$, contributes to transport identically. For propagating waves, from the graphene (lattice) Schrödinger equation, we obtain $d^b = ie^{i\varphi}d^a$, where $\tan\varphi = q_y/q_x$.

The interface equations, Eqs. (1), can be equivalently recast in the form of the wave-function matching, which is convenient when considering more complex scattering, such as NGN (see below). This can be done by continuing the wave functions across the interface and introducing fictitious wave-function elements $c_1$ and $d^b_{-1}$. The first two equations of Eqs. (1) become

$$t' d_0^a = t_s c_1, \quad t_g d^b_{-1} = t' c_0.$$

These are general boundary conditions and can be applied to a scattering problem with arbitrary arrangements. For example, scattering from N to G can be obtained if we use

$$c_0 = 1 + r, \quad c_1 = e^{ik_s a_s} + re^{-ik_s a_s}, \quad d^b_{-1} = d^b_0 e^{-ik_g a_g}.$$

Substituting into the above boundary conditions, we find the equations connecting the amplitudes of the waves,

$$t_s(e^{ik_s a_s} + re^{-ik_s a_s}) = t' d_0^a, \tag{3}$$

$$t'(1 + r) = t_g d_0^b e^{-ik_g a_g}. \tag{4}$$

Thus, for the reflection coefficient $R = |r|^2$, at low energies ($k_g a_g \ll 1$), we find

$$R = \frac{\beta + \beta^{-1} - 2\sin(\varphi + k_s a_s)}{\beta + \beta^{-1} - 2\sin(\varphi - k_s a_s)}, \quad \beta \equiv \frac{t'^2}{t_s t_g}. \tag{5}$$

Near half-filling, $k_s a_s \approx \pi/3$; however, these results apply to the case of arbitrary filling, where $k_s a_s \neq \pi/3$. As anticipated, for an opaque interface $t'^2 \ll t_a t_s$, the reflection approaches 1. Note also that one can only match the wave vectors in the $y$ direction for a very limited set of wave vectors around $k_s a_s = \pi/3$; all other states are ideally reflected by the interface.

## III. NORMAL-METAL–GRAPHENE–NORMAL-METAL CONTACT: PROPAGATING AND EVANESCENT MODES

Consider now a graphene sheet of length $L$ connected to two square-lattice metal electrodes (with the same overlap integral $t_s$) at two ideal zigzag interfaces. Note that such an arrangement is only possible provided $L = a_g(3N+1)/2$, with an integer $N$. For an odd-integer $N$, the square lattice leads are aligned [Fig. 2(b)]; for an even-integer $N$, they are shifted by half a period [Fig. 2(c)]. Note that sites at the two interfaces always belong to different graphene sublattices. We describe both cases on equal footing.

We take the wave function in the left electrode in the same form as before, $c(\boldsymbol{r}) = (e^{ik_s x} + re^{-ik_s x})e^{ik_y y}$, the wave function in graphene as a combination of left- and right-moving waves for each sublattice, and the wave function in the right electrode as the transmitted wave $f(\boldsymbol{r}) = w\exp(ik_s[x - L) + ik_y y]$.

The equations for the NGN structure read

$$t' c_0 = t_g(d_l^b + d_r^b)_{-1}, \tag{6}$$

$$t_s c_1 = t'(d_l^a + d_r^a)_0, \tag{7}$$

$$t' f_0 = t_g(d_l^a + d_r^a)_{(3N+1)/2}, \tag{8}$$

$$t_s f_{-1} = t'(d_l^b + d_r^b)_{(3N+3)/2}. \tag{9}$$

In addition to $c_1$ and $d^b_{-1}$, we introduced two more "unphysical" amplitudes, $d^a_{(3N+3)/2}$ and $f_{-1}$. We use now $d_r^b = -ie^{i\varphi}d_r^a$ and $d_l^b = ie^{-i\varphi}d_l^a$, where $\varphi$ in both expressions is defined for the right-moving electrons. Solving this scattering problem for $qa_g \ll 1$, we find for the transmission amplitude

$$w = -2i\cos\varphi \sin k_s a_s e^{ik_s a_s} J^{-1},$$

$$J = \beta^{-1}e^{-ik_s a_s}\cos(\varphi - qL\cos\varphi) - 2\sin(qL\cos\varphi) - \beta e^{ik_s a_s}\cos(\varphi + qL\cos\varphi). \tag{10}$$

Note that for $qL \ll 1$ and $t'^2 = t_s t_g$, the junction is ideally transmitting.

For a finite length of the graphene strip, there are also solutions which are not propagating, but rather exponentially increasing or decreasing as $e^{\pm\eta_x x}$—the *evanescent states*. Their energy reads

$$E_\pm = \pm\frac{3t_g}{2}\sqrt{q_y^2 - \eta_x^2},$$

which is defined as far as $|\eta_x| \leq |q_y|$. Similar to the propagating case, we can find the relation between the components of the graphene wave function,

$$d^b = \pm\sqrt{\frac{q_y + \eta_x}{q_y - \eta_x}}d^a, \tag{11}$$

where $\pm$ correspond to $E_\pm$. In the following, we consider the positive energy branch, $E_+$. While there is no propagation in the evanescent case, we can still define the right ($\eta_x > 0$) and left ($\eta_x < 0$) components of the wave function—the wave "propagates" in the direction of decay. For these components, $d_r^b = Zd_r^a$ and $d_l^b = Z^{-1}d_l^a$, where $Z = \sqrt{(q_y + |\eta_x|)/(q_y - |\eta_x|)}$. The transmission amplitude through the evanescent modes becomes

$$w = -2i \sinh\zeta \sin k_s a_s e^{ik_s a_s} \tilde{J}^{-1},$$

$$\tilde{J} = \beta^{-1} e^{-ik_s a_s} \sinh(\eta_x L + \zeta) - 2 \sinh \eta_x L + \beta e^{ik_s a_s} \sinh(\eta_x L - \zeta), \quad (12)$$

with $\zeta = \ln Z$. Clearly, for $t_g t_s = t'^2$ and $\eta_x L \ll 1$, we obtain again the perfect transmission.

## IV. CURRENT AND CONDUCTANCE

The current through the junction is expressed as

$$I_x = eW \int \frac{dk_s dk_y}{(2\pi)^2} v_x |w(k_s,k_y)|^2 = \frac{eW}{(2\pi)^2 \hbar} \int_{eV_G}^{eV_G+eV} dE \int dk_y |w(k_s,k_y)|^2, \quad (13)$$

where $W$ is the width of the graphene strip in the $y$ direction, and $v_x = \hbar^{-1} \partial E_s / \partial k_s$ is the group velocity. This expression includes the contribution from both propagating (real $k_s$) and evanescent (purely imaginary $k_s$) states.

Let us first consider the contribution of *propagating states*. The integration is carried over the momenta for which $v_x > 0$. In the linear regime, from Eq. (13), we obtain the conductance

$$\frac{G_{tr}}{G_Q} = \frac{W q_G}{\pi} \int_{-\pi/2}^{\pi/2} |w|^2 \cos\varphi d\varphi, \quad (14)$$

with $q_G \equiv 2e|V_G|/3t_g a_g$ and $G_Q = e^2/2\pi\hbar$ being the conductance quantum. Below, we analyze Eq. (14) analytically in the two limiting cases, short ($q_G L \ll 1$) and long ($q_G L \gg 1$) junctions.

For short junctions, $q_G L \ll 1$, the transmission coefficient,

$$|w|^2 = \frac{4\beta \sin^2 k_s a_s}{\beta^{-1} + \beta - 2\cos k_s a_s},$$

does not depend on the angle $\varphi$, and we obtain

$$\frac{G_{tr}}{G_Q} = \frac{2W q_G}{\pi} \frac{4\beta \sin^2 k_s a_s}{\beta^{-1} + \beta - 2\cos k_s a_s}. \quad (15)$$

The quantity $2W q_G/\pi$ can be interpreted as the "number of transport channels." In the case $\beta = 1$, the conductance equals $2W q_G G_Q/\pi$.

For long junctions, $q_G L \gg 1$, we use the fact that $\cos(q_G L \cos\varphi)$ is a rapidly oscillating function of the angle $\varphi$. In particular, for $\beta = 1$, we have

$$|w|^2 = \cos^2\varphi \sin^2 k_s a_s [\sin^2 k_s a_s \cos^2\varphi \cos^2(q_G L \cos\varphi) + (1 - \cos k_s a_a \sin\varphi)^2 \sin^2(q_G L \cos\varphi)]^{-1}. \quad (16)$$

In this situation, the integral in Eq. (13) can be discretized. Indeed, between the points $\varphi_n$ and $\varphi_{n+1}$, such that $\cos\varphi_n = \pi n / q_G L$, the integral in Eq. (13) can be easily calculated assuming that the slow functions $\cos\varphi$ and $\sin\varphi$ are constant and equal to $\cos\varphi_n$ and $\sin\varphi_n$ everywhere except for combination $\cos(q_G L \cos\varphi)$. Then Eq. (13) becomes a discrete sum over the periods $n$ of the function $\cos(q_G L \cos\varphi)$. Converting the sum into an integral (the integrand is a smooth function of $n$), one obtains

$$\frac{G_{tr}}{G_Q} = \frac{W q_G (1 - \sin k_s a_s)}{4 \sin k_s a_s \cos^2 k_s a_s}. \quad (17)$$

This result is length independent, similar to Eq. (15), and for $k_s a_s = \pi/3$, the conductance of a long graphene layer is suppressed as compared to a short layer.

For untransparent interfaces, $\beta \ll 1$, the transmission coefficient can be approximated as

$$|w|^2 = \frac{4\beta^2 \sin^2 k_s a_s \cos^2\varphi}{\cos^2(q_G L \cos\varphi - \varphi) + 4\beta^2 \sin^2 k_s a_s \sin^2(q_G L \cos\varphi)}. \quad (18)$$

This expression has the structure similar to that of resonant tunneling for a double barrier: Typically, the numerator is of order $\beta^2 \ll 1$, whereas the denominator is of order 1, and the transmission probability is small. However, for certain directions $\varphi_m$ of the wave vector, when the cosine in the denominator vanishes, the transmission becomes ideal. One can expand the expression around the resonance $\varphi_m$ to obtain the Breit-Wigner structure of the resonance, $\varphi = \varphi_m + \delta\varphi$, $\delta\varphi \ll 1$,

$$|w|^2 = \frac{4\beta^2 \sin^2 k_s a_s \cos^2\varphi_m}{(q_G L \sin\varphi_m - 1)^2 \delta\varphi^2 + 4\beta^2 \sin^2 k_s a_s \cos^2\varphi_m}. \quad (19)$$

Typically, one can omit 1 as compared to $q_G L \sin\varphi_m$ in the denominator. The main contribution to the current comes from the directions around the resonances ($\varphi$ close to $\varphi_m$). Integrating the Breit-Wigner expression (19) and transforming the resulting sum over $m$ into an integral, we obtain

$$G_{tr}/G_Q = \beta W q_G \sin k_s a_s. \quad (20)$$

Note that here the conductance of a long layer is proportional to $\beta$, and thus, parametrically exceeds the conductance of a short layer [proportional to $\beta^2$, Eq. (15)]. This effect is due to the resonant structure of Eq. (18).

Let us turn now to the contribution of the *evanescent modes*. In the vicinity of the Dirac point, the number of propagating states vanishes proportionally to $E$, and thus, the contribution of the large number of evanescent states with $|\eta_x| \approx |q_y|$ becomes dominant. At zero energy, $E \approx +0$, and $q_y > 0$, one has $Z \to \infty$. Thus, Eq. (12) becomes

$$w_+ = \frac{-2i \sin k_s a_s e^{ik_s a_s}}{\beta^{-1} e^{-ik_s a_s} e^{\eta_x L} - \beta e^{ik_s a_s} e^{-\eta_x L}}. \quad (21)$$

Interestingly, for negative values of the deviation $q_y < 0$ from the $K$ Dirac point, the transmission amplitude for zero-energy states ($E \approx +0$ and $Z \to 0$) is different,

$$w_- = \frac{-2i \sin k_s a_s e^{ik_s a_s}}{\beta^{-1} e^{-ik_s a_s} e^{-\eta_x L} - \beta e^{ik_s a_s} e^{\eta_x L}}. \quad (22)$$

Although for $\beta = 1$ the probabilities are the same, $|w_-|^2 = |w_+|^2$, for $\beta \neq 1$, they are different. This effect is related to the chirality of graphene Dirac fermions. A zigzag edge of

graphene supports a continuum of chiral edge states at zero energy:[14] They can only propagate in the direction $q_y>0$ for the lower Dirac point $K'$, and in the direction $q_y<0$ for the upper Dirac point $K$. These states decay exponentially into the bulk of graphene. In a graphene nanoribbon, which is essentially our graphene sheet disconnected from the electrodes, these states become evanescent modes[15] with exponentially small energies. It is this chiral nature of the surface states that causes an asymmetry between the two directions of $q_y$ in transmission.

Note that the expression for $w_-$ can be obtained from $w_+$ by flipping the sign of $\eta_x$; thus, integration over positive and negative values of $q_y$ in the conductivity is equivalent to integration over positive and negative values of $\eta_x$. The tunneling probability is

$$|w|^2 = \frac{4\sin^2 k_s a_s}{\beta^{-2}e^{2\eta_x L} + \beta^2 e^{-2\eta_x L} - 2\cos 2k_s a_s}. \tag{23}$$

It becomes ideal for $\beta=\exp(\eta_x L)$.

The conductance including now both Dirac points is

$$\frac{G_{ev}}{G_Q} = \frac{W}{\pi L}\int_{-\infty}^{+\infty} d\eta_x |w|^2 \tag{24a}$$

$$= \frac{W(\pi - 2k_s a_s)}{\pi L}\tan k_s a_s. \tag{24b}$$

Surprisingly, we find that the resulting conductivity is independent of the value of $\beta$, even for small $\beta$ (weak contact between the metal and graphene)! By inspection, one can see that in this limit the major contribution comes from $w_-$, i.e., the negative values of $q_y$. In the limit $\beta\ll 1$, the graphene region reduces to the zigzag nanoribbon, which, as mentioned above,[15] has a continuum of surface states for $q_y<0$; the conductivity is dominated by the tunneling through these states. A similar effect was discussed in Ref. 16 for tunneling between a carbon nanotube and a metallic electrode.

Still, Eq. (24b) clearly cannot hold for $\beta=0$. To establish the limits of its applicability, we analyze the terms that were dropped while going from Eq. (12) to Eqs. (21) and (22). Taking the limit $\zeta\to\pm\infty$ is only valid for exact zero-energy states. However, for finite transport or gate voltage such that $q_G\ll 1/L$, $Z(q_y<0)\approx q_G/|q_y|$. The conductivity Eq. (24b) is dominated by terms with $|q_y|\approx|\eta_x|\sim 1/L$. The subdominant terms in Eq. (12) therefore become non-negligible when $q_G>\beta/L$. Thus, the $\beta$-independent expression (24b) only holds for low enough transport and gate voltages, such that $q_G<\beta/L$. In this regime, our result agrees with the one obtained by Schomerus[13] for $\beta=1$.

To analyze the intermediate regime $\beta\ll q_G L\ll 1$, we keep for $q_y<0$ the leading term $\beta^{-1}\exp(-ik_s a_s+\eta_x L-\zeta)$ in the denominator of Eq. (12). This term only dominates provided $\eta_x$ is not too small, such that $\exp(\eta_x L)\gg 2\eta_x/q_G$. The solution of this transcendental equation, which in the leading order becomes $\eta_x=-L^{-1}\ln(q_G L/2)$, provides the cutoff in the integral over $\eta_x$ in the expression for the conductance. Explicitly, we have

TABLE I. Functional dependence on the parameters $q_G$, $L$, and $\beta=t'^2/t_s t_g$ of contributions to the conductance from propagating and evanescent modes in different transport regimes.

| | | Propagating | Evanescent |
|---|---|---|---|
| $\beta=1$ | $q_G\ll 1/L$ | $q_G$ | $L^{-1}$ |
| | $q_G\gg 1/L$ | $q_G$ | $L^{-1}(q_G L)^{-3}$ |
| $\beta\ll 1$ | $q_G\ll\beta/L$ | $q_G\beta^2$ | $L^{-1}$ |
| | $q_G\ll 1/L$ | $q_G\beta^2$ | $\beta^2 L^{-1}(q_G L)^{-2}\ln^2(q_G L)$ |
| | $q_G\gg 1/L$ | $q_G\beta$ | $\beta^2 L^{-1}(q_G L)^{-3}$ |

$$\frac{G_e v}{G_Q} = \frac{16W\beta^2}{\pi L(q_G L)^2}\ln^2(q_G L)\sin^2 k_s a_s.$$

Thus, away from zero energy, the contribution of evanescent modes rapidly vanishes, and conductance becomes proportional to $\beta^2$.

For yet greater gate voltages, $q_G L\gg 1$, the conductance is always dominated by the states with $\eta_x L\lesssim 1$. From $q_y^2-\eta_x^2=q_G^2$, we therefore find that at any rate $|q_y|\gg|\eta_x|$, and thus, $\zeta=\eta_x/q_G\ll\eta_x L$. This means that we can disregard $\zeta$ in the denominator of Eq. (12), and in the numerator, we replace $\sinh\zeta$ with $\eta_x/q_G$. Writing $dk_y\approx\eta_x d\eta_x/q_G$, we find that the integrand in the expression for the conductance contains the third power of $\eta_x$ multiplied with $e^{-\eta_x L}$. Consequently, we obtain

$$\frac{G_{ev}}{G_Q} = \frac{12\zeta(3)W}{\pi L(q_G L)^3}\frac{\sin^2 k_s a_s}{|\beta^{-1}e^{-ik_s a_s}+\beta e^{ik_s a_s}-2|^2}. \tag{25}$$

Here, $\zeta(n)$ is the zeta function, with $\zeta(3)\approx 1.2021$.

The results for the conductance in different regimes are shown in Table I.

## V. CONCLUSIONS

We constructed the wave-function matching conditions at the zigzag interfaces between square (N) and graphene (G) lattices, and determined transport properties of the NGN structure, concentrating on the regimes of "ideal" interface ($t'^2=t_a t_s$) and highly resistive interface ($t'^2\ll t_a t_s$). In accordance with earlier studies,[11,13] at the Dirac point, the conductance is dominated by the evanescent modes and scales inversely proportionally with the length of the contact $L$. However, the situation changes qualitatively as soon as one departs from the Dirac point, for instance, by changing the electron concentration via the gate voltage $V_G$. The propagating modes start to contribute to the conductance. For small $V_G$, such that $q_G L\ll 1$, their contribution is length independent; in particular, we find that for ideal interfaces, the transmission equals 1 independently of the angle of incidence. Further yet from the Dirac point, $q_G L\gg 1$, the conductance is determined by the propagating modes, whereas the evanescent modes' contribution decays as $L^{-4}$. In particular, for $q_G L\gg 1$ and $t'^2\ll t_s t_g$, we found a regime similar to resonant tunneling in double-barrier structures. As a consequence, the propagating modes' contribution of a long junction in this

case is greater than the one for a short junction.

We found that the contribution of evanescent modes at the Dirac point does not depend on $\beta$, but diminishes as we apply the gate voltage. In the regime $q_G L \gg 1$, this contribution is suppressed.

Besides looking at the low transport bias regime considered above, it also may be interesting to study the nonlinear $I-V_t$ characteristics. Our results suggest that with increasing transport voltage $V_t$, the contribution of the evanescent modes to the current saturates with voltage beyond $V_t > t_g a_g / L$, while the propagating modes' contribution increases as $V_t^2$. However, the quantitative discussion of the nonlinear regime is problematic, since the result would essentially depend on the potential distribution in contacts and over the graphene sheet. Investigation of this potential distribution would require the solution of the Poisson equation coupled to the equation for the particle density, and goes beyond the scope of this paper.

The zigzag interface considered in this paper is the simplest case of a contact: The periods of the lattices match, $a_s = \sqrt{3} a_g$, and the momentum component $k_y$ along the interface is conserved. In real experimental situations, both of these conditions will be difficult to realize: the interfaces are disordered, and the lattice periods may be incommensurate. This paper illustrates the importance of the interface contribution to the transport and provides the basis for future research in this direction.

*Note added*. At first glance, the result (25) disagrees with Ref. 13, which finds $G_{ev} \propto L^{-1}$ for all gate voltages. However, the chemical potentials in Ref. 13 were arranged in a different way than we have done it above: The chemical potential of graphene sheet is fixed to the Dirac point, whereas chemical potentials in the normal metal are varied. Recently, a study of nonlinear transport by Robinson and Schomerus has been made available.[17] Both our above results and the results of Ref. 13 follow in appropriate limiting cases.

## ACKNOWLEDGMENTS

We thank S. Trugman and H. Schomerus for useful discussions. We acknowledge Aspen Center for Physics, where this research was initiated. This work was supported in part by U.S. DOE.

[1] K. S. Novoselov, A. K. Geim, S. V. Morozov, D. Jiang, Y. Zhang, S. V. Dubonos, I. V. Grigorieva, and A. A. Firsov, Science **306**, 666 (2004).

[2] Y. Zhang, Y.-W. Tan, H. L. Stormer, and P. Kim, Nature (London) **438**, 201 (2005).

[3] E. Rollings, G.-H. Gweon, S. Y. Zhou, B. S. Mun, J. L. McChesney, B. S. Hussain, A. V. Fedorov, P. N. First, W. A. de Heer, and A. Lanzara, J. Phys. Chem. Solids **67**, 2172 (2006); X. Wu, X. Li, Z. Song, C. Berger, and W. A. de Heer, Phys. Rev. Lett. **98**, 136801 (2007).

[4] H. B. Heersche, P. Jarillo-Herrero, J. B. Oostinga, L. M. K. Vandersypen, and A. F. Morpurgo, Nature (London) **446**, 56 (2007).

[5] V. V. Cheianov and V. I. Fal'ko, Phys. Rev. B **74**, 041403(R) (2006); M. I. Katsnelson, K. S. Novoselov, and A. K. Geim, Nat. Phys. **2**, 620 (2006).

[6] M. I. Katsnelson, Eur. Phys. J. B **51**, 157 (2006); B. Trauzettel, Ya. M. Blanter, and A. F. Morpurgo, Phys. Rev. B **75**, 035305 (2007).

[7] Y. Zheng and T. Ando, Phys. Rev. B **65**, 245420 (2002).

[8] E. McCann, K. Kechedzhi, V. I. Fal'ko, H. Suzuura, T. Ando, and B. L. Altshuler, Phys. Rev. Lett. **97**, 146805 (2006).

[9] C. W. J. Beenakker, Phys. Rev. Lett. **97**, 067007 (2006).

[10] N. M. R. Peres, A. H. Castro Neto, and F. Guinea, Phys. Rev. B **73**, 195411 (2006).

[11] J. Tworzydlo, B. Trauzettel, M. Titov, A. Rycerz, and C. W. J. Beenakker, Phys. Rev. Lett. **96**, 246802 (2006).

[12] Recently, the existence of ripples at the surface of suspended graphene sheets has been reported, see J. C. Meyer, A. K. Geim, M. I. Katsnelson, K. S. Novoselov, T. J. Booth, and S. Roth, Nature (London) **446**, 60 (2007). The role of these ripples in electron scattering requires further investigation, and goes beyond the scope of this paper.

[13] H. Schomerus, Phys. Rev. B **76**, 045433 (2007).

[14] K. Nakada, M. Fujita, G. Dresselhaus, and M. S. Dresselhaus, Phys. Rev. B **54**, 17954 (1996).

[15] L. Brey and H. A. Fertig, Phys. Rev. B **73**, 235411 (2006).

[16] T. Nakanishi and T. Ando, J. Phys. Soc. Jpn. **69**, 2175 (2000).

[17] J. P. Robinson and H. Schomerus, Phys. Rev. B **76**, 115430 (2007).